Supplementary Methods

[^{11}C]PIB PET:

[^{11}C]PIB PET data were acquired as described in a previous study.[1] Briefly, data were acquired for 90 minutes (58 time frames) following an injection of 539 MBq (428 – 660 MBq) and reconstructed using 3-dimensional filtered back projection with corrections applied for randoms, dead time, normalization, scatter, attenuation and sensitivity. There was no significant difference in the injected activity for the control and TBI groups (554 $\pm$ 16 MBq vs. 528 $\pm$ 62 MBq; p=0.11).

In 7 TBI subjects and 4 controls we obtained 18 blood samples via a radial artery cannula (6 $\times$ 20s, 3min, 4min, 5min, 7min, 10min, 15min, every 10min thereafter). Radioactivity concentration in both whole blood and plasma was measured in a gamma well counter. Seven blood samples were used to determine the radio-labelled metabolite fraction in plasma (3min, 6min, 10min, 20min, 45min, 60min, 75min after injection). Concentrations of hydrophilic metabolites and [^{11}C]PIB were determined by solid-phase extraction of plasma.[2] For each subject, the metabolite fraction data were fitted with the Hill function[3] to derive a metabolite-corrected plasma input function. The metabolite-corrected plasma input function was used in conjunction with the Logan graphical method[4] to assess whether tissue equilibrium conditions were achieved within the scan duration, especially in white matter due to the slower kinetics.[5] In addition, in patients and control subjects for whom arterial blood samples were available, regional distribution volume ratio (DVR) calculated from reference tissue modelling was compared to the ratio of target and reference tissue distribution volumes (V_T) determined from plasma input Logan analysis.

A 65% threshold was applied to the smoothed probability maps to segment grey and white matter ROIs (Supplementary Fig 1). A threshold of 65% was chosen for initial segmentation as a compromise between maximizing ROI volume and making each ROI as homogeneous as possible in terms of the contribution made by grey or white matter to the ROI PET signal. To confirm the validity of this approach we explored the hypothesis that all of the observed increase in cortical [^{11}C]PIB binding was simply the consequence of contamination of the ROI signal by partial volume error from white matter voxels. To do this we modelled the effect of the calculated contamination from white matter voxels (using measured levels of white matter [^{11}C]PIB DVR obtained in individual patients) on a background of grey matter [^{11}C]PIB DVR values that were assumed to be identical to control mean values, and compared the values obtained by this modelling process to measured values in TBI patients. In addition, we repeated the entire analysis described above with grey/white segmentation undertaken using a threshold of 75% (Supplementary Fig 1).

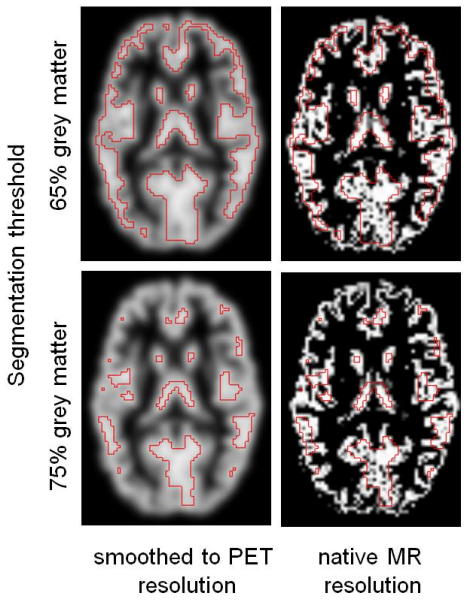

Supplementary Fig 1. The left panels show the grey matter probability map from T1 weighted MR image, smoothed to PET resolution, with ROIs defined in red using a 65% (above) and 75% (below) grey matter threshold. The right panels show the same ROIs on the grey matter probability map at native MR resolution.

Autoradiography and immunocytochemistry

Briefly, tissue blocks were dissected from a coronal slice of the fresh, unfixed brain at the level of the lateral geniculate nucleus. These blocks were then frozen in isopentane at -40°C and stored at -80°C until required. Blocks used in this study were selected to include: medial temporal lobe including the hippocampus, cingulate gyrus and adjacent corpus callosum, and thalamus. From these blocks, a series of 8μm cryostat sections were cut and prepared for either immunocytochemistry or autoradiography.

Immunocytochemistry: Following fixation in acetone for 10 minutes, sections were immersed in Avidin/Biotin Blocking Kit (Vector Laboratories, Burlingame, CA, USA), followed by blocking serum (normal horse serum; Vectastain Universal Elite Kit, Vector Labs). Sections were then incubated in primary antibody for 20h at 4°C. Immunostaining for β-amyloid was performed with a monoclonal antibody directed to the N-terminal epitope amino acid residues $A\beta/_{8-17}$ (clone 6F/3D; Dako, Carpinteria, CA, USA; 1:75), or with a monoclonal antibody specific to amyloid precursor protein (clone 22C11; Millipore, Billerica, MA, USA; 1:50,000). Visualization was achieved using a DAB kit (Vector Labs), following which the sections were scanned using a digital slide scanner (NanoZoomer; Hamamatsu, Hertfordshire, UK) and viewed using the SlidePath Tissue IA system (Dublin, Ireland).

Autoradiography: Sections were thawed to room temperature prior to 3 consecutive 5 min incubations in phosphate buffer saline (PBS, pH7.4) at 4°C. Slides were then incubated in PBS containing 10% ethanol and 0.5nM N-methyl-[^{3}H]2-(4'-methylaminophenyl)-6-hydroxybenzothiazole ([^{3}H]-PIB, Perkin Elmer LAS, UK) for 1 hour at room temperature. Non-specific binding was determined in the presence of 10μM BTA-1 (Sigma Aldrich, UK) in adjacent sections. After

incubation with radioligand, sections were washed for 2 x 30s in PBS at 4^0C and then 30 s in distilled water at 4^0C. Sections were dried in air before exposure to Kodak Biomax MR film.

Supplementary Results and Discussion:

1. Logan plot kinetic analysis in TBI compared to controls

The metabolite-corrected plasma input function in conjunction with the Logan graphical method suggested that equilibrium was achieved in both grey and white matter, and in both subject groups (controls and patients) at similar time points after tracer administration (Supplementary Fig 2). We plotted the correlation between DVR values obtained from Logan plots derived in two ways (with plasma input and reference tissue input) in TBI subjects for whom blood samples were obtained (n=7) and healthy controls for whom such data were available in our centre (n=5). Correlation was good in both subject populations (Supplementary Fig 3). The reference tissue method that we used has been previously validated in healthy subjects, and it was not our intention to repeat this validation in healthy controls with such a small number of subjects. However, our TBI data show concordance between the two derivations of DVR in 28 large regions in seven subjects with varying DVR values, and show that the slope of the relationship is similar to that seen in 16 regions from four healthy volunteers with DVR values that vary across a similar range. The inference that we draw from these data are that our results cannot easily be explained by differences in Logan plot performance in the TBI population.

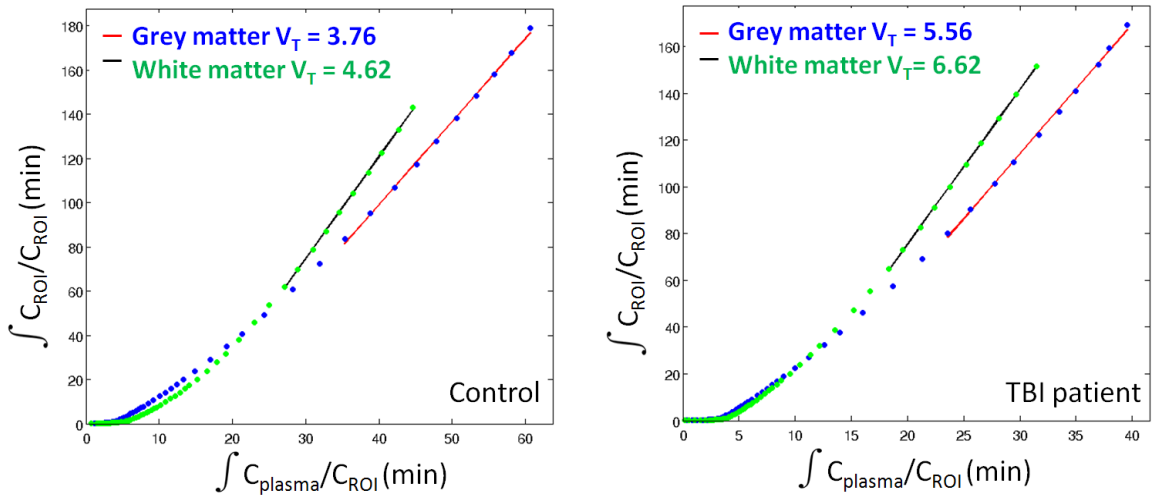

Supplementary Fig 2. Logan plots of [^{11}C]PIB PET data from a control subject (left) and a patient with TBI (right) achieve linearity, implying equilibration of the tracer in both grey and white matter during 90 minutes of data acquisition. C_{plasma}: Metabolite-corrected radioactivity concentration in plasma; C_{ROI}: Radioactivity concentration in region of interest; V_T: Total distribution volume.

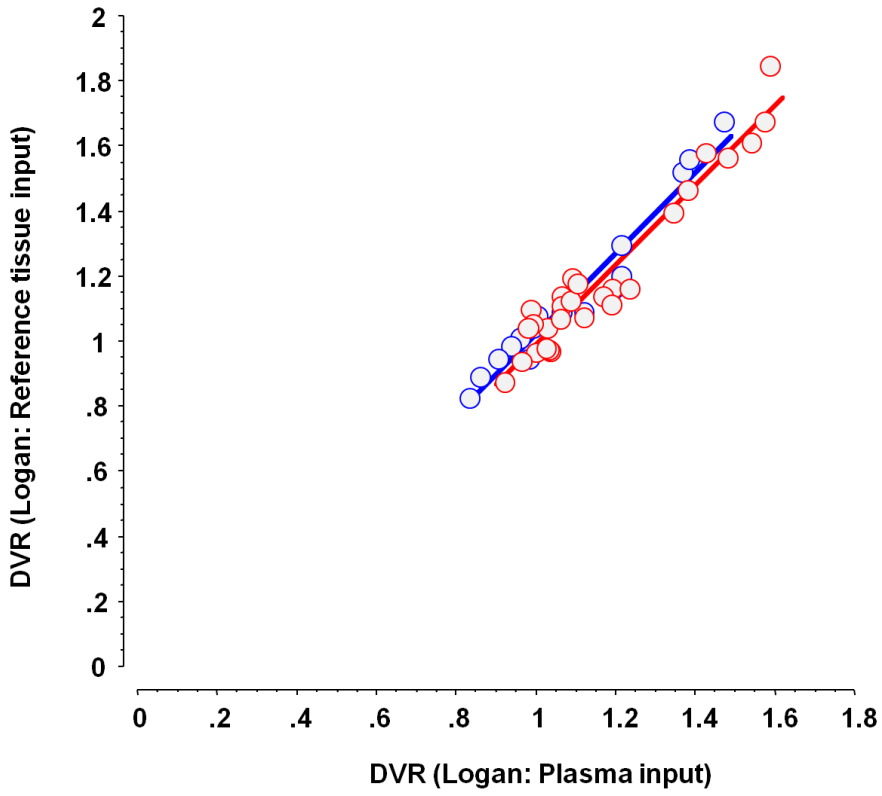

Supplementary Fig 3. Plot of DVR derived using Logan plot analysis: with plasma input on x axis *vs.* reference tissue on y axis. Separate data points are shown for cortical grey matter, striatum, thalamus and white matter ROIs in controls (n = 4; in blue) and TBI patients (n=7; in red). Separate regression lines are shown for controls (in blue; y = 1.24 x - 0.22; $p < 0.001$, r^2: 0.95) and patients with TBI (in red; y = 1.22 x - 0.23; $p < 0.001$, r^2: 0.93).

2. Partial volume error: Effect on grey matter ROI analysis

Given the fact that white matter DVR values were higher than grey matter in both controls and patients, we considered whether the increase in grey matter DVR observed in patients might have been a consequence of white matter signal spill-in into grey matter ROIs, i.e. partial volume error. However, the 65% threshold applied to the smoothed probability maps, combined with Lucy-Richardson deconvolution of the emission data, resulted in good separation of grey and white matter signals. The estimated contribution of white matter voxels to the cortical grey matter ROI values in the control and TBI groups was 9.3 $\pm$ 0.7 % and 9.1 $\pm$ 0.1 %, respectively. In order to determine whether such contamination could account for the increased cortical [^{11}C]PIB binding that we observed in TBI, we plotted observed DVR against a calculated value of DVR which assumed that all subjects had cortical DVR values equal to the control mean value plus a DVR contribution due to 10% of the white matter signal, using individual values for white matter DVR for such calculation. This showed that the observed increases in cortical grey matter DVR could not be accounted for by white matter contamination (Supplementary Fig 4, left panel). A similar analysis confirmed that the increase in striatal DVR seen in the TBI subjects could not be accounted for by contamination from white matter (which was estimated to be 9.1 $\pm$ 0.7% and 9.7 $\pm$ 1.2% in control and TBI subjects, respectively).

Using a 75% threshold for segmentation resulted in even smaller levels of contamination by white matter voxels in the cortical grey matter ROI values (5.9 $\pm$ 0.6% and 6.3 $\pm$ 0.3% in control and TBI subjects, respectively). This more stringent threshold tended to exclude areas of cortical grey matter in some patients (see Supplementary Figure 1, lower panels) but median [range] cortical grey matter [^{11}C]PIB DVR in the TBI patients remained nearly identical (0.99 [0.93-1.20] *vs.* 1.00 [0.94-1.18] for the 65% and 75% thresholds, respectively). Further, intergroup differences between control and TBI subjects were retained in the more strictly segmented data, with similar statistical differences between groups (p = 0.006 *vs.* 0.005). Again, modelling the measured contamination by white matter voxels (~6%) could not account for the increased cortical [^{11}C]PIB DVR seen in the TBI patients (Supplementary Fig 4, right panel).

Next, we considered whether our calculated white matter contamination of ~6% for the 75% threshold might have been an underestimate, and undertook a sensitivity analysis assuming levels of contamination at twice and four times this level. However, inter-group differences in cortical grey matter [^{11}C]PIB DVR in data segmented at a 75% tissue threshold remained significant even when we corrected for estimated contamination from white matter voxels with the extent of contamination set artificially high at 12% or 24% (p < 0.01 and < 0.05, respectively).

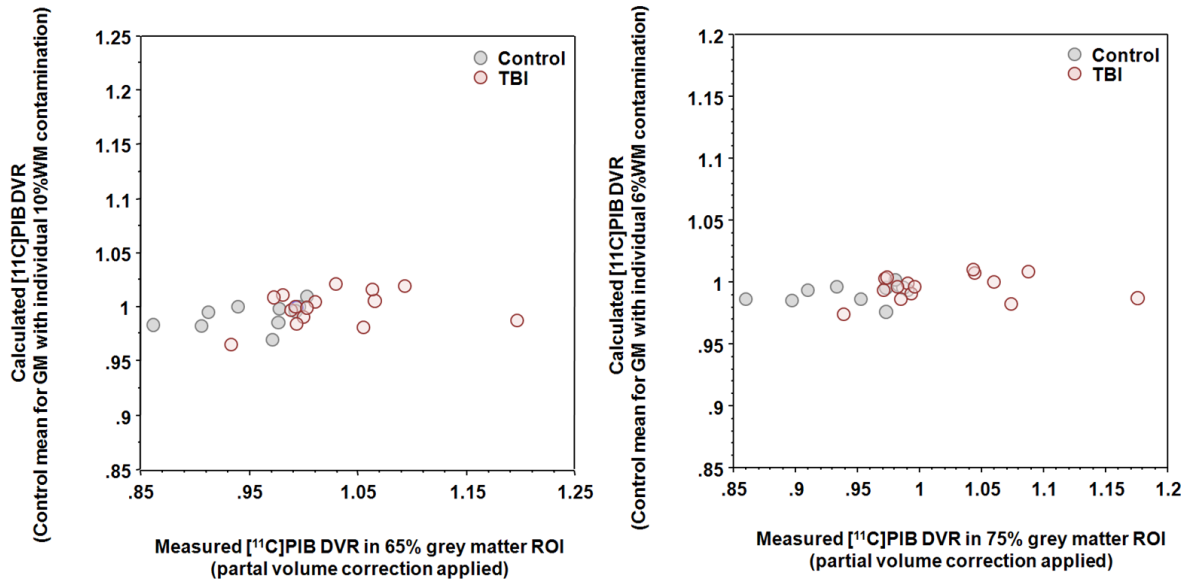

Supplementary Fig 4.
Left panel: Plot of observed cortical [^{11}C]PIB DVR for segmentation with a threshold of 65% applied to the smoothed grey matter probability map and application of Lucy-Richardson deconvolution (on x axis) plotted against a modelled cortical DVR value (on y axis) equal to the mean cortical grey matter [^{11}C]PIB DVR value observed in controls plus a 10% signal contamination from white matter voxels (using subject specific values for WM [^{11}C]PIB DVR). The modelled values for both controls (0.97-1.01) and TBI subjects (0.97-1.02) span a narrow range and are very similar (p = 0.19), while observed [^{11}C]PIB DVR in controls (0.86-1.00) and TBI subjects (0.93-1.20) vary across a wide range of values and are highly significantly different between the groups (p = 0.006).
Right panel: As for the left panel but for a threshold of 75% with a corresponding 6% signal contamination from white matter voxels. As for the 65% threshold, the modelled values in both controls (0.98-1.00) and TBI subjects (0.97-1.01) span a narrow range and are very similar (p = 0.19), while observed [^{11}C]PIB DVR in controls (0.86-1.00) and TBI subjects (0.94-1.18) vary across a wide range of values and are highly significantly different between the groups (p = 0.005).

3. Blood brain barrier disruption as a potential artifactual cause of increased [^{11}C]PIB binding in TBI

Finally, we undertook analysis to determine whether the increased [^{11}C]PIB DVR we observed in patients may have been the consequence of changes in blood-brain barrier (BBB) function in TBI. To do this, we compared kinetic parameters determined from metabolite-corrected plasma two tissue compartmental modeling (4 kinetic parameters plus blood volume) for controls (n=4) and patients (n=6) imaged at early time points, for which BBB disruption is most likely to have been a factor. We specifically looked for differences in $(K_1/k_2)/(K_1'/k_2')$ where K_1 and k_2 represent bidirectional transport of radiotracer across the BBB, and K_1' and k_2' represent the same parameters for the reference tissue region – the cerebellum in this case.[6] The term $(K_1/k_2)/(K_1'/k_2')$ is the ratio of the free distribution volumes in the target and reference tissues; this has previously been used to assess whether kinetic analysis using a reference tissue is being affected by BBB dysfunction.[7] This analysis, shown below in Supplementary Table 1 and Supplementary Fig 5, revealed no differences in $(K_1/k_2)/(K_1'/k_2')$ between healthy controls and TBI patients.

Region	Subject group	Mean	SD	CoV (%)	*p* (TBI vs. controls)
Cortical grey matter	Controls	0.896	0.093	10.7	0.98
	TBI patients	0.993	0.126	14.1	
Striatum	Controls	1.079	0.093	8.6	0.66
	TBI patients	1.118	0.173	15.5	

Supplementary Table 1. $(K_1/k_2)/(K_1'/k_2')$ for ROIs with significant differences in [^{11}C]PIB DVR in patients (cortical grey matter and striatum).

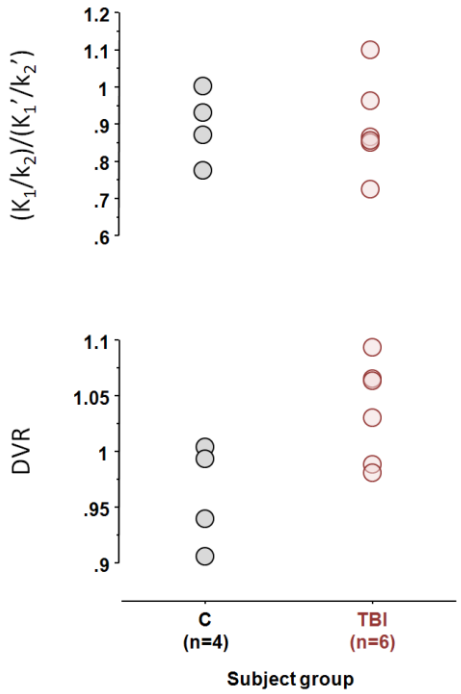

Supplementary Fig 5. Plot of individual values for $(K_1/k_2)/(K_1'/k_2')$ (above) and DVR (below) in cortical grey matter from controls (C) and TBI patients (TBI). The figure shows that the DVR values in the two groups are different, despite overlapping values of $(K_1/k_2)/(K_1'/k_2')$. Note that some of the values from TBI subjects are superimposed.

In addition, no increases in [^{11}C]PIB DVR were seen in pericontusional regions, which, in our patients, represented the region of most prominent BBB disruption and vasogenic oedema. Further supportive evidence that BBB disruption, or abnormal ligand transport in the presence of a preserved BBB, are unlikely to be important drivers of radioligand kinetics comes from two further sources outside our study.

First, two studies have now shown that [^{11}C]PIB is not a substrate for carrier mediated transport by human P-glycoprotein (P-gp, ABCB1) or breast cancer resistance glycoprotein (ABCG2) across the BBB,[8,9] negating the concern that damage to these transport mechanisms in TBI would hinder egress of the radioligand from the brain, leading to an increase in distribution volume.

Second, partial evidence that BBB disruption does not increase PET measures of [^{11}C]PIB binding comes from a study that used [^{11}C]PIB PET as a biomarker of amyloid clearance in AD patients treated with Aβ binding human monoclonal antibodies, which are known to produce vasogenic oedema at high dose. Ostrowitzki et al[10] reported that [^{11}C]PIB binding was reduced acutely in areas of vasogenic oedema in two patients following high dose gantenerumab, at a time when MR imaging showed clear evidence of BBB leak. Clearly, this finding is confounded by the fact that the intervention with gantenerumab may have cleared amyloid and reduced [^{11}C]PIB binding, but it at least shows that BBB dysfunction does not have a dominant effect on the estimation of [^{11}C]PIB binding in the brain.

Supplementary References:

1. Landt J, D'Abrera JC, Holland AJ, Aigbirhio FI, Fryer TD, Canales R, Hong YT, Menon DK, Baron JC, Zaman SH. Using positron emission tomography and carbon 11-labeled Pittsburgh compound B to image brain fibrillar β-amyloid in adults with Down syndrome: safety, acceptability, and feasibility. Arch Neurol 2011; 68: 890-6.
2. Barré L, Debruyne D, Abadie P, Moulin M, Baron JC. Methods for 11C-RO 15 1788 radioactive metabolite assay in rabbit, baboon, and human blood. Int J Appl Adiat Isot A 1991; 42: 435–439.
3. Gunn RN, Sargent PA, Bench CJ, Rabiner EA, Osman S, Pike VW, Hume SP, Grasby PM, Lammertsma AA. Tracer kinetic modeling of the 5-HT1A receptor ligand [carbonyl-^{11}C]WAY-100635 for PET. Neuroimage 1998; 8: 426-440.
4. Logan J, Fowler JS, Volkow ND, et al. Graphical analysis of reversible radioligand binding from time-activity measurements applied to [N-11C-methyl]-(-)-cocaine PET studies in human subjects. J Cereb Blood Flow Metab 1990; 10: 740-747.
5. Fodero-Tavoletti MT, Rowe CC, McLean CA, Leone L, Li QX, Masters CL, Cappai R, Villemagne VL. Characterization of PiB binding to white matter in Alzheimer disease and other dementias. J Nucl Med 2009; 50: 198-204.
6. Price JC, Klunk WE, Lopresti BJ, et al. Kinetic modelling of amyloid binding in humans using PET imaging and Pittsburgh Compound-B. J Cerebral Blood Flow Metab 2005; 25: 1528-1547.
7. Folkersma H, Boellaard R, Vandertop WP, Kloet RW, Lubberink M, Lammertsma AA, van Berckel BN. Reference tissue models and blood-brain barrier disruption:lessons from (R)-[11C]PK11195 in traumatic brain injury. J Nucl Med 2009; 50:1975-9.
8. Tournier N, Valette H, Peyronneau A-M, et al. Transport of selected PET radiotracers by human P-glycoprotein (ABCB1) and breast cancer resistance protein (ABCG2): An in vitro screening. J Nucl Med 2011; 52: 415-423.
9. Ishiwata K, Kawamura K, Yanai K, Hendrikse NH. In vivo evaluation of P-glycoprotein modulation of 8 PET radioligands used clinically, J Nucl Med 2007; 48:81–87
10. Ostrowitzki S, Deptula D, Thurfell L, et al. Mechanism of amyloid removal in patients with Alzheimer disease treated with gantenerumnab. Arch Neurol 2011; 69: 198-207.